

Cite this article as: Ba Zhixin, Kuang Juan, Ding Yuping, et al. Influence of Working Current Density on Formation and Corrosion Resistance of Super-Hydrophobic Coating on ZK60 Magnesium Alloy[J]. Rare Metal Materials and Engineering, 2022, 51(06): 1942-1948.

ARTICLE

# Influence of Working Current Density on Formation and Corrosion Resistance of Super-Hydrophobic Coating on ZK60 Magnesium Alloy

Ba Zhixin<sup>1,2</sup>, Kuang Juan<sup>1,3</sup>, Ding Yuping<sup>1</sup>, Zhao Fei<sup>1</sup>, Zhang Lingling<sup>1</sup>, Wang Yongmin<sup>1,2</sup>

<sup>1</sup> School of Materials Science and Engineering, Nanjing Institute of Technology, Nanjing 211167, China; <sup>2</sup> Jiangsu Key Laboratory of Advanced Structural Materials and Application Technology, Nanjing Institute of Technology, Nanjing 211167, China; <sup>3</sup> School of Materials Science and Engineering, Southeast University, Nanjing 211189, China

**Abstract:** To improve the corrosion resistance of magnesium alloys, super-hydrophobic (SH) coating was fabricated on the surface of ZK60 magnesium alloy coated with layered double hydroxides (LDHs) film. The electric field was introduced in the coating preparation process, and the influences of working current density on the characteristics of the coatings were researched. The results indicate that the working current densities significantly affect the microstructure of the LDHs films, which has an important impact on the hydrophobicity of the SH coatings. When the working current density is 25 mA/cm<sup>2</sup>, the SH coating presents a homogenous micro-nano structure and super-hydrophobicity. The corrosion current density of the SH coating ( $I_{\text{corr}} = 9 \times 10^{-7} \text{ A} \cdot \text{cm}^{-2}$ ) is two orders of magnitude lower than that of the ZK60 substrate ( $I_{\text{corr}} = 3 \times 10^{-5} \text{ A} \cdot \text{cm}^{-2}$ ), indicating excellent corrosion resistance.

**Key words:** magnesium alloy; super-hydrophobic coating; working current density; corrosion resistance

As a new generation of biodegradable medical metal materials, magnesium (Mg) and its alloys with excellent biocompatibility and mechanical compatibility, have become ideal materials in the field of medical implants<sup>[1-3]</sup>. However, the overquick degradation rate of magnesium-based materials in the body environment severely limits their clinical development<sup>[4-6]</sup>. The construction of super-hydrophobic (SH) coating is one of the emerging methods that slow down the degradation rate of magnesium<sup>[7,8]</sup>.

At present, the preparation methods of super-hydrophobic surfaces include chemical etching, electrodeposition, chemical conversion coating, etc<sup>[9-11]</sup>. Zhao<sup>[12]</sup> studied the preparation of super-hydrophobic coating on the surface of AZ31 magnesium alloy in a solution containing ferric chloride and myristic acid (MA). Long-chain myristic acid can quickly impart hydrophobicity to the substrate surface and promote the formation of a biocompatible surface. The coating can effectively reduce the corrosion rate of the substrate in 3.5wt% NaCl solution.

Moreover, layered double hydroxides (LDHs) films have

been considered as promising alternative conversion coatings on magnesium alloys, based on the ion exchange characteristics of LDHs film<sup>[13-15]</sup>. In the corrosive environment, the LDHs films will release interlayer anions and adsorb Cl<sup>-</sup> to block the corrosion of corrosive ions and provide effective protection to the substrate<sup>[16]</sup>. LDHs film with high porosity and roughness are conducive to obtaining a super-hydrophobic surface<sup>[17]</sup>. Wang<sup>[18]</sup> fabricated an anti-corrosion super-hydrophobic coating by growing in-situ Mg-Al LDHs film with molybdate intercalation and lauric acid modification on AZ31 magnesium alloy. The synergistic effect of the physical properties of coating protection, corrosion inhibition effect of molybdate and super-hydrophobicity of lauric acid leads to corrosion resistance of the coating.

The electric field is one of the effective ways to improve the quality and control the structure of the film, such as micro-arc oxidation and anodization of magnesium alloys and some other alloys<sup>[19,20]</sup>. The electric field can adjust the polarization state of the sample surface and achieve the directional

Received date: August 18, 2021

Foundation item: National Natural Science Foundation of China (51701093); Qing Lan Project of Jiangsu Province of China

Corresponding author: Ba Zhixin, Ph. D., Professor, School of Materials Science and Engineering, Nanjing Institute of Technology, Nanjing 211167, P. R. China, Tel: 0086-25-86118276, E-mail: bzhx@njit.edu.cn

Copyright © 2022, Northwest Institute for Nonferrous Metal Research. Published by Science Press. All rights reserved.

movement of anions and cations to accelerate the reaction and control the structure of the coating<sup>[21]</sup>.

In this study, special micro-nano structure of LDHs film was fabricated on ZK60 magnesium alloy with the electric field assistance under different working current densities. The micro-nano structured film can be treated by low surface energy corrosion inhibitors (stearate acid, SA) to prepare a super-hydrophobic surface. The effects of working current density on the morphology, composition, wettability and corrosion resistance of the coatings were investigated. The essential connection between super-hydrophobicity and micro-nano structure was revealed.

## 1 Experiment

### 1.1 Coating preparation

The substrate materials were ZK60 magnesium alloy plates (composition: Zn 5wt%, Zr 0.3wt%, Mn 0.1wt% and the balance Mg, Northeast Light Alloy Co., Ltd) with a dimension of 15 mm×20 mm×5 mm. They were polished with increasing grades (600#, 1200# and 1500#) of silicon carbide papers. Then, the substrates were ultrasonically cleaned in ethanol and dried with cold air.

Subsequently, the substrates were acid-immersed in 0.025 mol/L MnCl<sub>2</sub> and HCO<sub>3</sub><sup>-</sup>/CO<sub>3</sub><sup>2-</sup> saturated carbonate solution for 2 h at 50 °C to provide Mg<sup>2+</sup> ions. The LDHs film formation was carried out in 0.5 mol/L Na<sub>2</sub>CO<sub>3</sub> electrolyte with auxiliary electric field at 50 °C. The specimen and the graphite plate were used as cathode and anode, respectively. The distance between the cathode and anode was 2 cm. To investigate the effect of working current density on coating preparation, the films were fabricated with different working current densities of 5, 25, and 50 mA/cm<sup>2</sup> by a direct current power supply for 1 h and then dried in air after washing by deionized water.

Continually, the LDHs samples were immersed into 0.1 mol/L stearate acid (SA) ethanol solution at 50 °C for 4 h. At last, the as-prepared samples were removed from the solution and dried in air at room temperature for further characterization. To well identify these samples, the pure LDHs films fabricated at the working current densities of 5, 25, and 50 mA/cm<sup>2</sup> were labeled as LDHs5, LDHs25 and LDHs50, and after modifying by stearate acid they were labeled as SH5, SH25 and SH50, respectively.

### 1.2 Characterization methods

Scanning electron microscopy (SEM, JSM-6360LV) was used to investigate the microstructure and surface morphology of the coatings. X-ray diffraction (XRD, UltimaIV, Rigaku) was used to characterize the crystal structure of the samples. attenuated total reflection Fourier transform infrared spectroscopy (ATR-FTIR, Nicolet IS 10) was employed to examine functional groups of the coatings.

The contact angles of the samples were tested with a contact angle meter (JY-82C). The values of the contact angles were calculated by the angle measurement way. The volume of simulated body fluid (SBF) drops was 3 μL in each test, the radius of which is definitely less than a capillary length, and

thus the droplet shape cannot be significantly affected by the gravity field<sup>[22]</sup>. The test was performed at different positions on the surface of the sample and the average of five measurements was taken as the final result. The SBF was composed of NaCl (8.0 g·L<sup>-1</sup>), KCl (0.4 g·L<sup>-1</sup>), NaHCO<sub>3</sub> (0.35 g·L<sup>-1</sup>), MgSO<sub>4</sub>·7H<sub>2</sub>O (0.2 g·L<sup>-1</sup>), CaCl<sub>2</sub> (0.14 g·L<sup>-1</sup>), Na<sub>2</sub>HPO<sub>4</sub> (0.06 g·L<sup>-1</sup>), KH<sub>2</sub>PO<sub>4</sub> (0.06 g·L<sup>-1</sup>) and glucose (1 g·L<sup>-1</sup>)<sup>[23]</sup>.

Potentiodynamic polarization and electrochemical impedance spectroscopy (EIS) tests were performed using an electrochemical workstation (PARSTAT 2273) to evaluate the electrochemical corrosion behavior of the samples. EIS plots were performed with an AC amplitude of 5 mV at open circuit potential by a frequency range from 100 mHz to 100 kHz. The collected EIS plots were fitted and analyzed by Zsimpwin software. The potentiodynamic polarization curves were measured from the potential of -1.9 V to -1.1 V at a scanning rate of 3 mV·s<sup>-1</sup>.

In addition, the coated samples were immersed in SBF at 37±0.5 °C, and the hydrogen released during the immersion process was collected through the gas collector above the inverted funnel. The immersion test was performed in triplicate. The hydrogen evolution rate (HER),  $V_H$  (mL·cm<sup>-2</sup>·h<sup>-1</sup>) can be calculated by Eq.(1).

$$V_H = V/st \quad (1)$$

where  $V$  denotes the hydrogen evolution volume,  $s$  and  $t$  are the exposed area of the sample and immersion time, respectively. Moreover, the corresponding corrosion rate  $P_H$  (mm·a<sup>-1</sup>) was calculated based on hydrogen evolution curves according to Eq.(2)<sup>[22]</sup>.

$$P_H = 54.696V_H \quad (2)$$

## 2 Results and Discussion

### 2.1 Coating characterizations

The XRD patterns of the LDHs films and SH coatings are shown in Fig. 1. The characteristic peaks of Mg from the substrate material inevitably appear in the XRD patterns. For the LDHs films, the diffraction peaks near 11.5° and 23.1° are ascribed to the diffraction of Mg<sub>6</sub>Mn<sub>2</sub>(OH)<sub>16</sub>CO<sub>3</sub>·4H<sub>2</sub>O crystal faces (003) and (006) (JCPDS 44-1446), respectively. In addition, there are characteristic peaks of Mg(OH)<sub>2</sub> and MnCO<sub>3</sub> in the XRD pattern. When working current density is 5 mA/cm<sup>2</sup>, the peak strength of Mg in the film is strong, while the peak strength of Mg<sub>6</sub>Mn<sub>2</sub>(OH)<sub>16</sub>CO<sub>3</sub>·4H<sub>2</sub>O, Mg(OH)<sub>2</sub> and MnCO<sub>3</sub> is weak. The diffusion and growth of LDHs grains caused by increasing the current density lead the peak intensity of Mg<sub>6</sub>Mn<sub>2</sub>(OH)<sub>16</sub>CO<sub>3</sub>·4H<sub>2</sub>O to increase as LDHs25 sample showed. The existence of the electric field can change the polarization state of the sample surface. The sample is in the low potential region of the cathode, and the metal cations have higher activity on the sample surface. The applied current density causes the free electrons in the matrix to continuously gather on the surface of the matrix. The concentration of OH<sup>-</sup> ions and CO<sub>3</sub><sup>2-</sup> ions in the solution is relatively high, which provides alkaline conditions and sufficient anions for the film-forming reaction on the surface

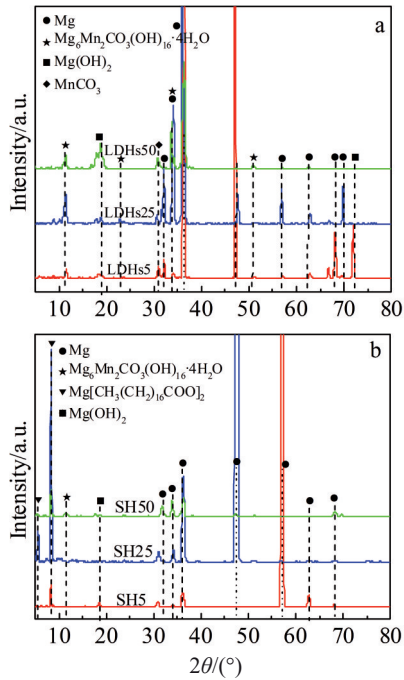
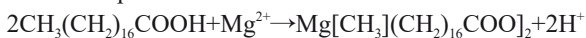


Fig.1 XRD patterns of the LDHs films (a) and SH coatings (b)

of the substrate. It promotes the migration of substances on the surface of the substrate and provides a driving force for the film-forming reaction of the LDHs film, so as to accelerate the film-forming reaction and change the structure and composition of the film. However, the content of Mg<sub>6</sub>Mn<sub>2</sub>(OH)<sub>16</sub>CO<sub>3</sub>·4H<sub>2</sub>O in the LDHs50 film decreases. The film has high hydrogen adsorption capacity at high current density, which will hinder the deposition of LDHs on the surface<sup>[23]</sup>.

After SA modification, the peaks near 6.3°, 8.5° correspond to the diffraction of magnesium stearate, which is the phase composition of the fabricated SH coatings. The specimen SH25 has the strongest characteristic peak of the magnesium stearate (Mg[CH<sub>3</sub>(CH<sub>2</sub>)<sub>16</sub>COO]<sub>2</sub>). It can be inferred that the following reaction occurs on the LDHs film during modification process.



FT-IR spectra of the SH coatings was used to further analyze the functional group structure of the coatings, as shown in Fig.2.

The wide absorption band at 3750~3060 cm<sup>-1</sup> corresponds to O-H stretching vibration. The band at 1370 cm<sup>-1</sup> originates from the symmetric and asymmetric stretching modes of CO<sub>3</sub><sup>2-</sup> which can be traced back to the CO<sub>3</sub><sup>2-</sup> in the film and atmospheric CO<sub>2</sub>. The absorption peaks at 2850, 2918 and 728 cm<sup>-1</sup> are caused by the C-H asymmetric and symmetric stretching vibrations, and -CH<sub>2</sub> stretching vibrations, respectively. The presence of COO<sup>-</sup> vibration at 1550 cm<sup>-1</sup> is related to magnesium stearate. The absorption peak strength of COO<sup>-</sup> is much stronger at the working current density of 25 mA/cm<sup>2</sup>, which indicates that the component content of magnesium stearate is higher.

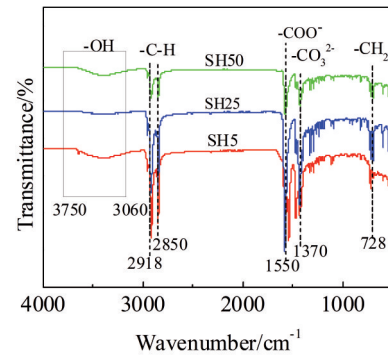


Fig.2 FT-IR spectra of the SH coatings

The current density affects the growth degree of the LDHs film on the surface of ZK60, which has a certain impact on the surface morphology of the SH coating. Fig.3 and Fig.4 show the SEM and 3D profiler images of the LDHs films and the corresponding SH coatings at different current densities. The working current density mainly affects the stacked sheet-like state of the LDHs films, so it shows different surface roughness. Sample LDHs5 shows a sparse flake structure with a roughness of 0.797 μm. When the working current density increases to 25 mA/cm<sup>2</sup>, the surface of the LDHs film is uniform and flat, composed of closely packed nano-sheet structures. The roughness of LDHs25 reduces to 0.618 μm. As the working current density continues to increase, the sheet-like LDHs pile up into blocks and the surface roughness increases, as shown in sample LDHs50. The SH coatings are clustered. The flaky structure and the surface roughness are obviously enlarged. There are many voids and cracks on the surface of SH5 and SH50, which is consistent with the surface morphology of LDHs films. While, SH25 with relatively large roughness benefits to coating hydrophobic improvement.

Fig. 5 shows the contact angles of LDHs films and SH coatings. The contact angles of LDHs5, LDHs25, LDHs50 film samples are 29.1° ± 3.5°, 17.6° ± 2.4° and 24.5° ± 5.1°, respectively, all less than 30°. After SA modification, the surface contact angles of the SH5, SH25, and SH50 samples are 146.2° ± 4.7°, 155.9° ± 3.1° and 150.1° ± 3.4°, respectively. In the process of SA modification, as the active molecule and amphoteric group, the hydrophilic end of SA is bound to the surface of the LDHs-coated ZK60 alloy, and the hydrophobic end is located on the outside, so that the fabricated surface exhibits hydrophobic characteristics. There are many grooves between the micro- and nano-layered structures on the surface of the film, and an air cushion forms in them. Since the size of the droplet is much larger than the surface micro-nano structure, the air cushion can effectively block the droplet when the droplet is in contact with the surface. The droplet cannot wet the surface and suspends above the rough structure, which greatly reduces the contact area between droplet and the coating. According to the Wenzel model, the increase in the surface roughness of the SH coating can make the coating more hydrophobic, so as to achieve super-

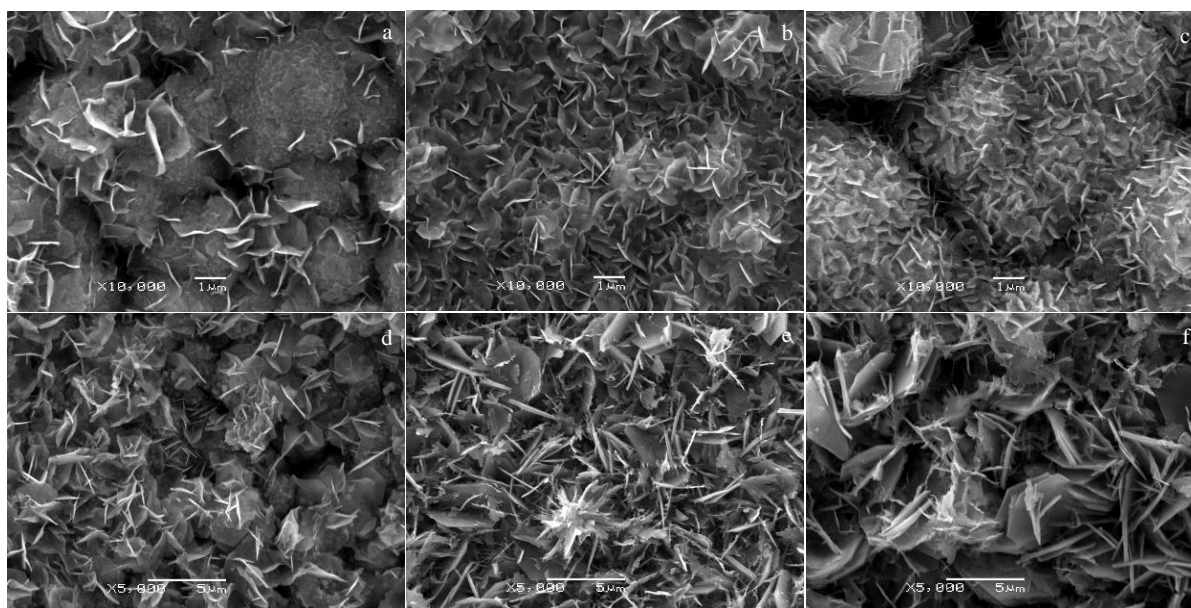


Fig.3 SEM images of the LDHs films and SH coatings: (a) LDHs5, (b) LDHs25, (c) LDHs50, (d) SH5, (e) SH25, and (f) SH50

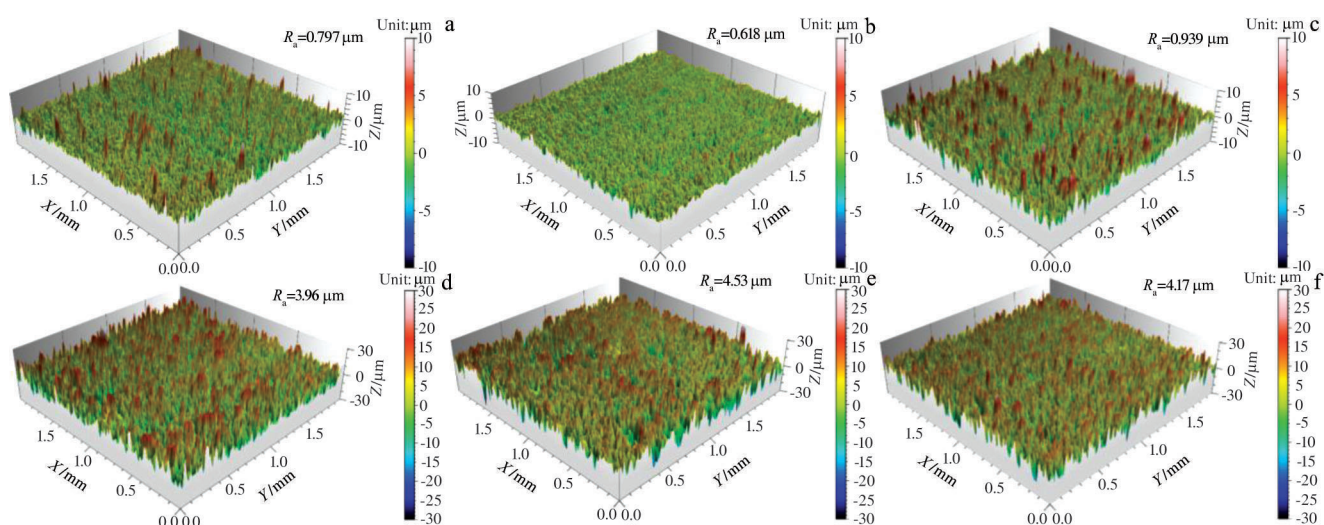


Fig.4 3D profiler images of the LDHs films and SH coatings: (a) LDHs5, (b) LDHs25, (c) LDHs50, (d) SH5, (e) SH25, and (f) SH50

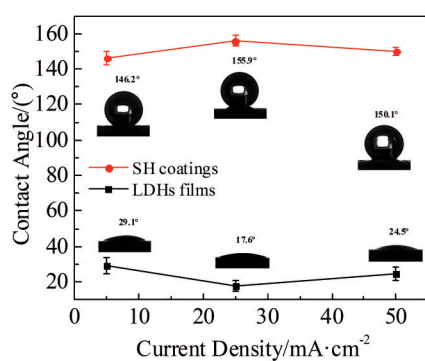


Fig.5 Contact angles of the LDHs films and SH coatings at different current densities

hydrophobic performance. When the working current density is  $25 \text{ mA}/\text{cm}^2$ , the micro-nano structure of the LDHs film and the hydrophobicity of magnesium stearate increase the contact angle. While a dense and uniform LDHs film has not been formed completely at the working current density of  $5 \text{ mA}/\text{cm}^2$ , resulting in poor hydrophobic performance of the SH coating after modification. In addition, when the working current density increases to  $50 \text{ mA}/\text{cm}^2$ , the growth of the LDHs film is hindered due to high hydrogen adsorption capacity. The SH coating obtained after modification still has a large number of pores, which provide a path for liquid immersion, and the hydrophobicity of the coating decreases.

## 2.2 Electrochemical corrosion behavior

Fig.6a shows the anodic and cathodic polarization curves of

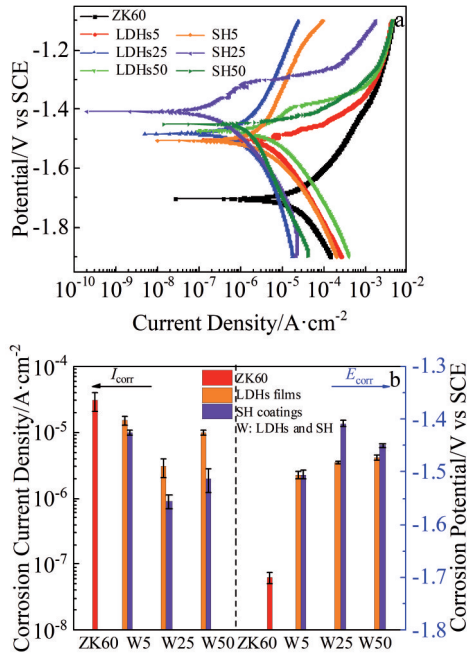


Fig.6 Polarization curves of ZK60, LDHs films and SH coatings in SBF (a) and relative electrochemical corrosion parameters (b)

ZK60, LDHs films and SH coatings in SBF, and the electrochemical corrosion parameters from polarization curves are listed in Fig.6b. Generally speaking, higher  $E_{corr}$  and lower  $I_{corr}$  indicate better corrosion resistance. The anode reaction is controlled by the oxidation and dissolution of the magnesium substrate, while the cathode reaction corresponds to the oxygen reduction reaction in the reduction process. The  $E_{corr}$  and  $I_{corr}$  of the ZK60 substrate are  $-1.71$  V and  $3 \times 10^{-5} \text{ A} \cdot \text{cm}^{-2}$ , respectively. The  $E_{corr}$  of the LDHs film and the SH coating samples is higher than that of the uncoated ZK60, and the  $I_{corr}$  is lower than that of the uncoated ZK60. The  $I_{corr}$  of the LDHs25 sample is  $3 \times 10^{-6} \text{ A} \cdot \text{cm}^{-2}$ , which is lower than that of LDHs5 and LDHs50. That is, the LDHs film fabricated under the working current density of  $25 \text{ mA/cm}^2$  has the best corrosion resistance among LDHs samples. Compared with the LDHs films, the SH coatings obtained by SA immersion can reduce  $I_{corr}$  and improve corrosion resistance. With increasing the working current density, the  $I_{corr}$  values of the SH coatings firstly decrease and then increase. Among them, the  $E_{corr}$  value of the sample SH25 is the highest, reaching  $-1.41$  V, and the  $I_{corr}$  value is the smallest, reaching  $9 \times 10^{-7} \text{ A} \cdot \text{cm}^{-2}$ , which is two orders of magnitude lower than that of uncoated ZK60 sample. Therefore, it can be preliminarily concluded that the prepared SH coatings can effectively block the penetration of corrosive ions in the electrolyte.

Corrosion resistance of the bare and coated ZK60 plates was further analyzed using the electrochemical impedance spectroscopy (EIS), as shown in Fig.7 (the points represent the experimental data while the lines display the fitting results). EIS results were fitted with the equivalent circuit models, as shown in Fig.8. The fitting element parameters are listed in

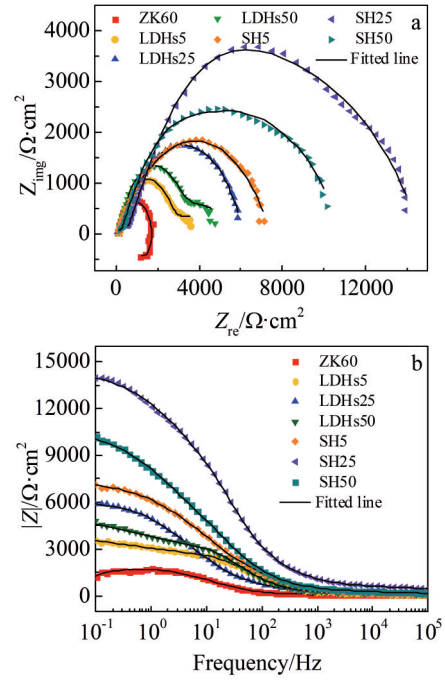


Fig.7 Nyquist plots (a) and Bode impedance plots (b) of ZK60, LDHs films and SH coatings in SBF

Table 1. In the circuits,  $R_s$ ,  $R_{ct}$ ,  $R_f$  and  $R_c$  represent the solution resistance, the charge-transfer resistance, the film resistance, and the SH coating resistance, respectively.  $Q_{dl}$  is the capacitance of the double-layer.  $Q_f$  is the constant phase element that simulates the capacitance of the oxide film and LDHs film.  $C_c$  indicates the capacitance of the SH coating. In addition, the inductive behavior corresponds to the resistance ( $R_l$ ) and inductance ( $L$ ) in series, indicating that pitting corrosion occurs on the surface of the uncoated ZK60 plate at the low frequency. When the dissolved oxygen in the corrosion solution increases, Mg will be passivated. However, the chloride ion ( $\text{Cl}^-$ ) has a strong penetrating power to metal, and can be selectively adsorbed on the passivation film (oxide film) of the metal, replacing oxygen atoms. Failure of the oxide film leads to pitting corrosion, which eventually leads to

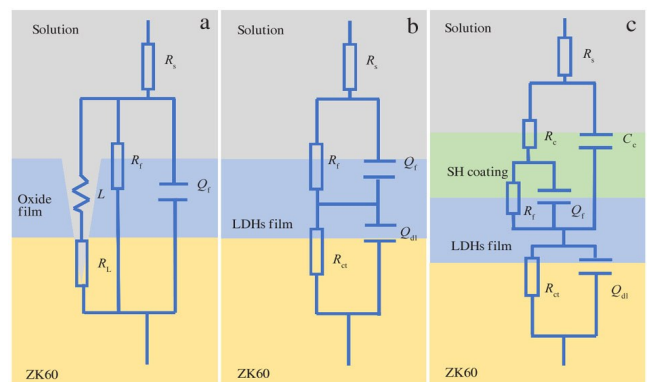


Fig.8 Equivalent electrical circuits of ZK60 (a), LDHs films (b) and SH coatings (c)

**Table 1** Fitting element parameters of EIS plots

Sample	$R_s/$ $\Omega \cdot \text{cm}^2$	$R_c/$ $\Omega \cdot \text{cm}^2$	$R_f/$ $\Omega \cdot \text{cm}^2$	$R_{ct}/$ $\Omega \cdot \text{cm}^2$
ZK60	92.15	-	1678	1299
LDHs5	84.03	-	2109	2517
LDHs25	62.49	-	2742	5796
LDHs50	84.09	-	3391	2319
SH5	83.26	52.05	7071	237.1
SH25	109.6	388.7	10010	4408
SH50	116.4	123.2	8880	1867

aggravation of local corrosion. The semicircle in the low frequency range reflects the response of the double electric layer, which determines the corrosion resistance of the sample. Generally, the larger the arc, the better the corrosion resistance. It can be observed that the arc of the SH coatings is much larger than that of the ZK60 substrate. Furthermore, the  $|Z|_{0.1\text{Hz}}$  value of samples increases after preparation with LDHs film and further modification with SA according to the Bode impedance plots (Fig. 7b). The SH coating with working current density of  $25 \text{ mA/cm}^2$  exhibits the largest  $R_f + R_{ct}$  and  $|Z|_{0.1\text{Hz}}$ . For superhydrophobic surfaces, due to the presence of air pockets and capillary forces, the corrosive medium is not easy to penetrate the metal surface. In addition, the micro/nano cavities and trapped air behave like the dielectric of a parallel plate capacitor. Air can weaken the transfer ability of electrons between electrolyte and the substrate, thereby improving the corrosion resistance of the substrate.

Fig. 9 displays the hydrogen evolution and corresponding

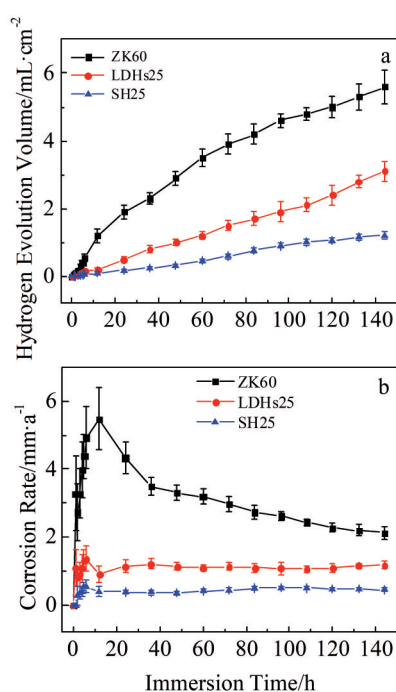


Fig.9 Hydrogen evolution curves (a) and corresponding corrosion rate (b) of ZK60, LDHs films and SH coatings in SBF

corrosion rate curves of ZK60, LDHs films and SH coatings in SBF. The ZK60 plate is exposed to corrosive solutions without coating protection, resulting in rapid hydrogen release during the initial immersion stage. With the extension of the immersion time, the hydrogen evolution rate (HER) slightly decreases. At this stage, corrosion products are formed to protect the ZK60 plate from rapid corrosion. As for the LDHs coated sample, the HER decreases obviously at the beginning due to the protection provided by LDHs film, and then the HER begins to increase because of the destruction of the LDHs film. Finally, the HER of the LDHs film sample slowly decreases and is stabilized due to the formation of corrosion products. The protective effect of the SH coating, which further inhibits the contact of corrosive media with the substrate, induces the lowest HER of the SH25 sample. It shows a slight upward trend in the first 6 h, then slightly decreases and finally maintains about  $0.5 \text{ mm} \cdot \text{a}^{-1}$ . The result indicates that SH coating possesses the best corrosion resistance, which is consistent with the result in Fig. 5 and Fig.6.

### 3 Conclusions

1) The electric field is introduced in the super-hydrophobic (SH) coating preparation process, and the working current density is the main factor that affects the coating performance.

2) The surface morphology and corrosion resistance of the layer double hydroxides (LDHs) film have a positive correlation with the formation of the SH coating. When the working current density is low, the coating with slow deposition speed has fine crystalline state, resulting in incomplete coating growth under the same processing time. However, too high current density will result in coarse coating structure.

3) The structure of the LDHs film is uniform and the corresponding SH coating has a static contact angle of  $155.9^\circ \pm 3.1^\circ$ , when the working current density is  $25 \text{ mA/cm}^2$ . The corrosion resistance of the SH coating ( $I_{\text{corr}} = 9 \times 10^{-7} \text{ A} \cdot \text{cm}^{-2}$ ) is significantly superior to that of the LDHs film ( $I_{\text{corr}} = 3 \times 10^{-6} \text{ A} \cdot \text{cm}^{-2}$ ) and the ZK60 substrate ( $I_{\text{corr}} = 3 \times 10^{-5} \text{ A} \cdot \text{cm}^{-2}$ ).

4) The hydrogen evolution rate (HER) of the SH25 coated sample after 144 h immersion reaches  $0.5 \text{ mm} \cdot \text{a}^{-1}$ , which provides effective corrosion resistance to the ZK60 substrate.

### References

- 1 Chu X, Wang Z, Zhang T et al. *Rare Metal Materials and Engineering*[J], 2018, 47(5): 1429
- 2 Sezer N, Evis Z, Kayhan S M et al. *Journal of Magnesium and Alloys*[J], 2018, 6(1): 23
- 3 Shao Y, Zeng R C, Li S Q et al. *Acta Metallurgica Sinica, English Letters*[J], 2020, 33(5): 615
- 4 Dong Q, Zhou X, Feng Y et al. *Bioactive Materials*[J], 2021, 6(1): 158
- 5 Dalawai S P, Saad Aly M A, Lathe S S et al. *Progress in Organic Coatings*[J], 2020, 138: 105 381

- 6 Xie J, Hu J, Fang L et al. *Surface and Coatings Technology*[J], 2020, 384: 125 223
- 7 Zhang C L, Zhang F, Song L et al. *Journal of Alloys and Compounds*[J], 2017, 728: 815
- 8 Liu Y, Xue J, Luo D et al. *Journal of Colloid and Interface Science*[J], 2017, 491: 313
- 9 Yeganeh M, Mohammadi N. *Journal of Magnesium and Alloys* [J], 2018, 6: 59
- 10 Ishizaki T, Masuda Y, Sakamoto M. *Langmuir*[J], 2011, 27: 4780
- 11 Jiang D, Zhou H, Wan S et al. *Surface and Coatings Technology* [J], 2018, 339: 155
- 12 Zhao L, Liu Q, Gao R et al. *Corrosion Science*[J], 2014, 80: 177
- 13 Guo L, Wu W, Zhou Y et al. *Journal of Materials Science & Technology*[J], 2018, 34: 1455
- 14 Zhang G, Wu L, Tang A et al. *Advanced Materials Interfaces*[J], 2017, 4: 1 700 163
- 15 Sun J, Li S, Xu H et al. *Rare Metal Materials and Engineering* [J], 2020, 49(12): 4236
- 16 Wang F, Guo Z, *Journal of Alloys and Compounds*[J], 2018, 767: 382
- 17 Kuang J, Ba Z X, Li Z Z et al. *Applied Surface Science*[J], 2020, 501: 144 137
- 18 Wang X, Jing C, Chen Y et al. *Journal of Magnesium and Alloys* [J], 2020, 8: 291
- 19 Yang M, Tang N, Huang Tingyu et al. *Rare Metal Materials and Engineering*[J], 2020, 49(2): 404
- 20 Zhang S F, Hu G H, Zhang R F et al. *Transactions of Nonferrous Metals Society of China*[J], 2020, 20(2): 660
- 21 Li Z, Ba Z X, Wang T et al. *Surface Technology*[J], 2019, 48: 69
- 22 Mei D, Lamaka S V, Lu X et al. *Corrosion Science*[J], 2020, 171: 108 722
- 23 Zhang Z Q, Wang L, Zeng M Q et al. *Bioactive Materials*[J], 2020, 5: 398

## 电流密度对 ZK60 镁合金表面超疏水涂层的制备及耐腐蚀性的影响

巴志新<sup>1,2</sup>, 匡娟<sup>1,3</sup>, 丁玉萍<sup>1</sup>, 赵斐<sup>1</sup>, 张玲玲<sup>1</sup>, 汪永民<sup>1,2</sup>

(1. 南京工程学院 材料科学与工程学院, 江苏 南京 211167)

(2. 南京工程学院 江苏省先进结构材料与应用技术重点实验室, 江苏 南京 211167)

(3. 东南大学 材料科学与工程学院, 江苏 南京 211189)

**摘要:** 为了提高镁合金的耐腐蚀性能, 基于层状双氢氧化物 (LDHs) 膜在 ZK60 镁合金表面制备了超疏水 (SH) 涂层。涂层制备过程中引入电场辅助, 研究了工作电流密度对涂层性能的影响。结果表明, 工作电流密度显著影响 LDHs 膜的微观结构, 这对 SH 涂层的疏水性具有重要影响。当工作电流密度为 25 mA/cm<sup>2</sup> 时, SH 涂层表面呈现均匀的微纳米结构, 并表现出超疏水性。超疏水涂层的腐蚀电流密度 ( $I_{\text{corr}}=9\times 10^{-7} \text{ A}\cdot\text{cm}^{-2}$ ) 比 ZK60 基体的腐蚀电流密度 ( $I_{\text{corr}}=3\times 10^{-5} \text{ A}\cdot\text{cm}^{-2}$ ) 低了 2 个数量级, 表现出优异的耐腐蚀性。

**关键词:** 镁合金; 超疏水涂层; 工作电流密度; 耐腐蚀性

作者简介: 巴志新, 女, 1979 年生, 博士, 教授, 南京工程学院材料科学与工程学院, 江苏 南京 211167, 电话: 025-86118276, E-mail: bzhx@njit.edu.cn